Memory Effects Explain the Fractional Viscosity Dependence of Rates associated with Internal Friction: Simple Models and Applications to Butane Dihedral Rotation

Bikirna Roy,[1] V. M. Hridya,[1] and Arnab Mukherjee[1]
Department of Chemistry, Indian Institute of Science Education and Research Pune - 411008

(Dated: February 2024)

Barrier-crossing rates of biophysical processes, ranging from simple conformational changes to protein folding, often deviate from the Kramers prediction of an inverse viscosity dependence. In many recent studies, this has been attributed to the presence of internal friction within the system. In our previous work, we showed that memory-dependent friction arising from the non-equilibrium solvation of a single particle can also cause such a deviation and be misinterpreted as internal friction. Here, we show that, even in the absence of an explicit solvent, memory effects can arise from within the molecule due to the coupling of the reaction coordinate motion with frictionally orthogonal degrees of freedom. Further, we find that the strength of the coupling determines the extent of the deviation from Kramers Theory. We show this for not only a simple diatom model but also cis-trans isomerization rates of butane, establishing the generality of our results.

I. INTRODUCTION

Several biophysical phenomena, be it a simple conformational change in a small molecule like butane or as complex as protein folding, can be modeled as barrier-crossing processes along appropriate reaction coordinates. According to Transition State Theory (TST), the rates of such processes depend solely on the barrier height, E_b, and the frequency of the reactant well, ω_r, such that $k_{TST} = \frac{\omega_r}{2\pi} e^{-E_b/k_B T}$. However, it fails to account for the recrossing at the barrier top as a result of collisions with solvent molecules. Kramers' theory (KT) successfully accounts for these factors by incorporating a correction factor κ called the transmission coefficient.[1] In the overdamped limit, the transmission coefficient is equal to ω_b/ξ, where ω_b is the barrier frequency, and ξ is the solvent friction coefficient. Assuming the solvent friction to be purely hydrodynamic, i.e., $\xi = 6\pi\eta r$ and the barrier curvature to be independent of the viscosity, one would expect the rate to be inversely proportional to the viscosity (η). However, as early as the 1980s, Fleming and co-workers[2] found that the rates of photochemical isomerization of some simple organic molecules do not show an inverse viscosity dependence. Instead, these rates were found to follow a power law characterized by a fractional parameter α such that:

$$k \propto \frac{1}{\eta^{\alpha}} \qquad \alpha < 1 \tag{1}$$

In 1992, Ansari *et al.*[3] found that the solvent viscosity dependence of conformational change rates in myoglobin could be explained by the empirical relation:

$$k = \frac{C}{\eta + \sigma} \tag{2}$$

The σ term in Ansari's equation has since been used as a convenient measure of the solvent-independent dry friction or "internal friction" present in biophysical systems. Numerous experimental and theoretical studies have found that internal friction plays a key role in governing the rates of important biophysical processes, from the chain dynamics of intrinsically disordered proteins (IDPs)[4,5] to the unfolded state dynamics[4–6] and protein folding pathways[7–11]. Clarke and coworkers used internal friction (IF) to explain the differential folding rates of the R15, R16, and R17 domains of α-Spectrin despite their similar structures and thermodynamic stabilities.[11–13] Proteins that form α helices have been argued to have more IF, thereby justifying their slower folding rates compared to β hairpin forming peptides.[14–16] This is relevant in the context of neurodegenerative diseases, which involve the formation of misfolded beta sheets. However, the molecular origin of IF is still unclear, with explanations ranging from the formation of hydrogen bonds[10], concerted dihedral rotations[17] to increased dispersion interactions[18] and even landscape roughness[11].

After Ansari's equation, any deviation from Kramers' theory in barrier-crossing rates of biophysical processes has been attributed to internal friction. But in 1980, Grote and Hynes[19] showed that a breakdown of Kramer's theory can also result from friction on the reaction coordinate being non-Markovian. Grote-Hynes theory (GHT) describes the motion of a reaction coordinate q in a potential of mean force (PMF) of the form $G[q(t)]$ near the transition state using a Generalized Langevin Equation (GLE) as

$$\mu\ddot{q} = -\frac{\partial G[q(t)]}{\partial t} - \mu \int_0^t \xi(\tau)\dot{q}(t-\tau)d\tau + R(t), \tag{3}$$

where $\xi(t)$ (also called memory friction or memory

kernel) is a time-dependent friction resulting from the nonequilibrium solvation due to the rapid motion of the reaction coordinate across the barrier. μ is the effective mass of the reaction coordinate and $R(t)$ is a random fluctuating force such that $\langle R(t)R(t+\tau)\rangle = \mu k_B T \xi(t)$. The reaction coordinate experiences an effective friction $\xi(\lambda_r)$ that can be smaller than the full solvent friction, leading to higher barrier-crossing rates than expected from KT. Bagchi and Oxtoby[20] showed that incorporating memory-dependent friction could satisfactorily explain the fractional viscosity dependence of the rates observed by Fleming and co-workers[2].

Recently, Hridya *et al.* have demonstrated an example of such non-equilibrium solvent effects when discussing the origin of internal friction.[21] They have shown that a single particle that crosses a one-dimensional barrier in the presence of an explicit solvent shows a deviation from KT with a non-zero σ value (Eq. (2)) and, correspondingly, a α value less than 1 (Eq. (1)). However, since the particle has no "internal" coordinates, we realize that the fractional viscosity dependence in this case is purely a consequence of the breakdown of the Markovian approximation of Kramers' theory. The study showed that the viscosity dependence of the rate was in good agreement with the GHT, which includes memory-dependent friction[21].

Best and co-workers also argued that solvent memory effects could be a source of internal friction.[9]. Surely, such memory effects are not restricted only to the solvent, and they can arise from coupled motions within the system (be it a protein or a simple molecular solute) as well. A recent work by Netz *et al.*[22] has shown the role of memory effects (both solvent and internal) in governing the dihedral rotation of butane. Laage *et al* have also demonstrated that non-Markovian friction (from both protein and solvent) plays a key role in the loop opening and closing dynamics of the PTP1B enzyme[23].

In all of the previous studies, explicit solvent was used to demonstrate the effect of memory function while attributing the outcome (a deviation from the Kramers equation) to internal friction. The reason for attributing the deviation of the viscosity dependence of the rate from Kramers to internal friction is purely in the context of Ansari's equation, where an explicit solvent is considered. In this work, we show, with the help of simple models, that memory-dependent friction can arise even in the absence of explicit solvent solely from the coupling of internal motions. We argue that the so-called "internal friction", characterized by a fractional viscosity dependence of the rate, results from the friction becoming non-Markovian or memory-dependent. Additionally, our results demonstrate that the strength of the coupling determines the degree of fractional viscosity dependence and the extent of the deviation from Kramers' theory. Finally, we used this simple model to explain the memory effects present in the Gauche-Anti interconversion of butane in an implicit solvent.

II. A SIMPLE DIATOMIC MODEL

A. System Design

We construct a simple diatom model as shown in Figure 1. The particle A moves under the influence of the solvent while connected by a harmonic spring of frequency ω_c to particle 'B', which moves in the double-well potential $V(q)$ as shown below.

$$V(q) = \frac{V_o}{b^4}\left[\left(q - \frac{a}{2}\right)^2 - b^2\right] \tag{4}$$

Here, V_0 is the barrier height, $a/2$ is the location of the barrier top or transition state, and $2b$ is the separation between the two wells. For simplicity, we restrict the motion of the particles to one dimension only. The position of the second particle x_2 is our reaction coordinate of interest in this case. No other interaction exists between the particles except the harmonic spring that joins them. This model, as shown below, is a minimal extension, with just one additional degree of freedom, to the model used in the previous study of Hridya *et al.*[21], where one particle crosses a barrier along one dimension.

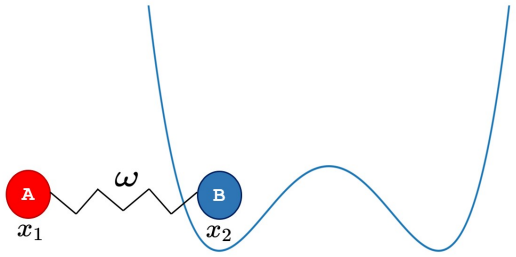

FIG. 1: Schematic representation of the diatom model in the double-well potential.

B. Non-Markovian (Memory) Friction

The particle 'A' experiences solvent friction, so we can write a Langevin equation to model its time evolution using mass-weighted coordinates. Since the particle 'A' is not the one actively crossing the potential energy barrier, we can think of its mass-weighted coordinate $m_1 x_1$ as a non-reactive coordinate and denote it as q_n.

$$\ddot{q}_n(t) = -\omega_c^2(q_n(t) - q_r(t)) - \xi\dot{q}_n(t) + R(t), \tag{5}$$

where ξ is the solvent friction coefficient in ps^{-1}, and ω_c is the coupling frequency. $R(t)$ is a random force that follows the Fluctuation Dissipation Theorem such that $\langle R(t)R(t^{'})\rangle = 2\xi k_B T\delta(t-t^{'})$.

For particle 'B', no such solvent friction is present. Instead, it moves in the double well potential $V(q)$ defined in equation (4). So its equation of motion can be written in terms of a mass-weighted reactive coordinate $q_r = m_2 x_2$ as:

$$\ddot{q}_r(t) = \omega_c^2(q_n(t) - q_r(t)) - \nabla V[q_r(t)] \quad (6)$$

Since the above two equations are coupled, we can write an equivalent generalized Langevin equation (GLE) for only the reactive coordinate q_r[24]. To do this, we must find $q_n(t)$ by solving the differential equation (5) and substituting it into the equation (6). We start by applying Laplace transforms on both sides of equation (5):

$$\mathcal{L}\{\ddot{q}_n(t)\} = \mathcal{L}\{-\omega_c^2 q_n(t) + \omega_c^2 q_r(t) - \xi\dot{q}_n(t) + R(t)\}$$

which evaluates to:

$$s^2\hat{q}_n(s) - sq_n(0) - \dot{q_n}(0) = \\ -\omega_c^2(\hat{q}_n(s) - \hat{q}_r(s)) - \xi[s\hat{q}_n(s) - q_n(0)] + \hat{R}(s),$$

where $\hat{q}_n(s)$ and $\hat{q}_r(s)$ are the Laplace transforms of $q_n(t)$ and $q_r(t)$ respectively. Similarly, $\hat{R}(s)$ is the Laplace transform of the random force. Rearranging, we get

$$\hat{q}_n(s) = \hat{q}_r(s) - \frac{s+\xi}{s^2+\omega_c^2+\xi s}[s\hat{q}_r(s) - q_r(0)] \\ + \frac{(\xi+s)[q_n(0) - q_r(0)] + \dot{q}_n(0) + \hat{R}(s)}{s^2+\omega_c^2+\xi s}$$

Following the work of Gertner, Wilson, and Hynes,[25] we can define the third term on the right-hand side as the Laplace transform of the effective random force on the non-reactive mode $\hat{R}_{eff}(s)$. Together, we can write

$$\hat{q}_n(s) = \hat{q}_r(s) - F(s)\,[s\hat{q}_r(s) - q_r(0)] + \hat{R}_{eff}(s), \quad (7)$$

where

$$F(s) = \frac{s+\xi}{s^2+\omega_c^2+\xi s}$$

Finally, the inverse Laplace Transform of equation (7) provides $q_n(t)$.

$$q_n(t) = q_r(t) - \mathcal{L}^{-1}\{F(s)\,[s\hat{q}_r(s) - q_r(0)]\} + R_{eff}(t)$$

Expressing the second term as a convolution, this can be rewritten as:

$$q_n(t) = q_r(t) - f(t) * \mathcal{L}^{-1}\{s\hat{q}_r(s) - q_r(0)\} + R_{eff}(t),$$

where $f(t)$ is the inverse Laplace Transform of $F(s)$ such that

$$f(t) = e^{-\xi t/2}\left[\cos(\gamma t) + \frac{\xi}{2\gamma}\sin(\gamma t)\right] \quad (8)$$

with $\gamma = \sqrt{\omega_c^2 - \xi^2/4}$.

Now we realize that $s\hat{q}_r(s) - q_r(0)$ is simply the Laplace transform of $\dot{q}_r(t)$. Hence

$$q_n(t) = q_r(t) - f(t) * \dot{q}_r(t) + R_{eff}(t) \quad (9)$$

Putting equation (9) in equation (6), we get

$$\ddot{q}_r(t) = -\nabla V[q_r(t)] - \omega_c^2\,[f(t) * \dot{q}_r(t)] + R_{eff}(t)$$

Finally, let us write out the convolution in terms of an integral so that we have

$$\ddot{q}_r(t) = -\nabla V[q_r(t)] - \omega_c^2 \int_0^t f(\tau)\dot{q}_r(t-\tau)d\tau + R_{eff}(t)$$

or

$$\ddot{q}_r(t) = -\nabla V[q_r(t)] - \int_0^t \xi_{eff}(\tau)\dot{q}_r(t-\tau)d\tau + R_{eff}(t) \quad (10)$$

This is the required GLE in the reactive mode coordinate q_r, where

$$\xi_{eff}(t) = \omega_c^2 f(t) \\ = \omega_c^2 e^{-\xi t/2}\left[\cos(\gamma t) + \frac{\xi}{2\gamma}\sin(\gamma t)\right] \quad (11)$$

Thus, coupling of the reactive coordinate motion to the nonreactive coordinate results in a non-Markovian or memory-dependent effective friction $\xi_{eff}(t)$ on the reactive coordinate. Note that the final expression for the memory-dependent friction does not depend on the nature of the potential energy surface in which the reaction coordinate is moving. Hence, we can extend this simple model to any realistic system, where we consider the reaction coordinate of interest to be coupled harmonically to one or more orthogonal degrees of freedom when moving under the influence of the solvent.

III. METHODS

To complement our analytical approach and validate the accuracy of our theoretical predictions, we performed molecular dynamics (MD) simulations of the diatomic model. The memory-dependent friction is extracted from these simulations, allowing for a direct comparison with the analytically derived kernel $\xi_{eff}(t)$. We examine the effect of the memory-dependent friction $\xi_{eff}(t)$ on the barrier crossing rates of the particle 'B' in the diatomic model and the solvent viscosity dependence of these rates. In addition, to extend our model to a realistic system, we calculate the cis-

trans isomerization rates of butane and extract the associated memory kernels from MD simulations of butane in solvents of varying viscosity.

A. Simulation Details

We carried out implicit solvent Langevin dynamics simulations for the diatomic model using the LAMMPS molecular dynamics software[26]. Since no explicit solvent is considered, the system has no solvent-memory effect. For a single particle crossing the one-dimensional barrier for such a system, the Kramers theory works as shown by Hridya *et al.*.[21]. The objective of the present study is to show the origin of the memory effect from the coupling of reactive and nonreactive degrees of freedom, even in the absence of the solvent. The viscosity of the medium was controlled by the damping time $1/\xi$ of the Langevin thermostat[27]. Here, ξ denotes the friction coefficient of the implicit solvent or the Langevin bath in ps^{-1}. All simulations were performed at 300K. We set the barrier height of the double-well potential $V(q)$ (see equation (4)) to 9 kJ mol^{-1} with the two wells located at 1.5 Å and 3.0 Å. The barrier frequency (ω_b) is 23.1 ps^{-1}.

To study the cis-trans isomerization of butane, we performed simulations of a united atom butane model using GROMACS 21.4[28]. We used the GROMOS 58 force field[29] for the butane molecule. All bonds and angles were constrained using the LINCS algorithm[30]. Here also, we performed Langevin dynamics simulations using the Stochastic Dynamics integrator at 300K. In GROMACS, the viscosity of the implicit solvent can be modulated using the coupling constant of the thermostat.

B. Mean First Passage Time (MFPT)

MFPT measures the average time τ for the transition from reactant to product. Hence, it is a direct method to calculate the barrier crossing rate. For the diatomic model, we calculated the time required for the spatial diffusion of particle 'B' across the barrier in the double-well potential $V(q)$ from multiple 5 ns long simulations. For butane, we ran 20 ns long simulations to measure the time required for the dihedral rotation from the cis to the trans isomer. We averaged the first passage times over 1000 replicas of both systems. We performed the MFPT calculations at different viscosities and fit them to the following heuristic relation to find α, which is a measure of the solvent viscosity dependence of the rate.

$$\frac{\tau}{\tau_0} = \left(\frac{\eta}{\eta_0}\right)^{\alpha} \tag{12}$$

Here τ_0 is the MFPT for the normal solvent viscosity η_0. Note that α is 1 for KT. A value of α less than unity signifies a deviation from Kramers' theory, often interpreted as internal friction. This indicates that the barrier-crossing process is less sensitive to the change in solvent viscosity than that in KT.

C. Memory Kernels from MD Simulations

As mentioned in Section I, the dynamics of the reaction coordinate (RC) can often be mapped to a GLE as in Equation (3). If we clamp the system at the Transition State (TS), then the first two terms in (3) become zero, and the random force $R(t)$ becomes equal to the total force on the reaction coordinate $F_{RC}(t)$. We can then evaluate the memory kernel using the second Fluctuation Dissipation theorem as,

$$\xi_{TS}(\tau) = \frac{\langle F_{RC}(t) F_{RC}(t+\tau)\rangle}{\mu k_B T} \tag{13}$$

This was achieved for the diatomic model by restraining the particle B fixed at the barrier-top at $x = 2.25$ Å. The forces acting along the RC were recorded every 0.1 fs for 1 ps long simulations. The effective mass of the reaction coordinate μ was evaluated from the mean square velocity of the RC in the transition state using the equipartition theorem[31]:

$$\frac{1}{2}\mu\langle v^2_{RC,TS}\rangle = \frac{1}{2}k_B T \tag{14}$$

Alternatively, we could extract the memory kernel without constraining the reaction coordinate at the transition state by employing a method originally outlined by Berne and Harp[32] and recently modified by Netz *et al.*[22] Multiplying the GLE in equation (3) by $\dot{q}(0)$ and taking ensemble average yields:

$$\mu\langle\dot{q}(0)\ddot{q}(t)\rangle = -\langle\dot{q}(0)\nabla G[q(t)]\rangle - \mu\int_0^t \xi_{eff}(\tau)\langle\dot{q}(0)\dot{q}(t-\tau)\rangle d\tau. \tag{15}$$

This is a Volterra integral equation, where we have utilized the fact that $\langle\dot{q}(0)R(t)\rangle = 0$. Discretizing this equation and replacing the integral with a summation using the trapezoidal rule, we find the following.

$$\xi_i = -\frac{1}{\mu C_0^{\dot{q}\dot{q}}\Delta t\omega_{i,i}}(\mu\sum_{j=0}^{i-1}\omega_{i,j}\xi_j C_{i-j}^{\dot{q}\dot{q}}\Delta t + \mu C_i^{\dot{q}\ddot{q}} + C_i^{\dot{q}\nabla G}) \tag{16}$$

Here, Δt is the discrete timestep, and ξ_i is the value of the friction kernel at the i^{th} timestep.

We define the correlation functions as, $C_i^{\dot{q}\dot{q}} = \langle \dot{q}(0)\dot{q}(i\Delta t)\rangle$, $C_i^{\dot{q}\ddot{q}} = \langle \dot{q}(0)\ddot{q}(i\Delta t)\rangle$, $C_i^{\dot{q}\nabla G} = \langle \dot{q}(0)\nabla G[q(i\Delta t)]\rangle$. $\omega_{i,j}$ is the integration weight of the trapezoidal rule. The initial value friction kernel, ξ_0, for the iteration can be calculated as

$$\xi_0 = \frac{-C_0^{\nabla U\ddot{q}} + \mu C_0^{\ddot{q}\ddot{q}}}{\mu C_0^{\dot{q}\dot{q}}} \tag{17}$$

We calculate the memory kernels for Butane using this method since it does not require us to constrain the reaction coordinate (in this case, the dihedral angle ϕ) at the transition state. We evaluated the PMF $G[\phi(t)]$ from the equilibrium probability density of the dihedral angle as $G[\phi] = -k_B T \log p(\phi)$.

D. Transmission Coefficients (TC)

The TST rate does not depend on the solvent viscosity since it is derived from static energy landscape[33]. Since the actual rate is $k = \kappa k_{TST}$, the transmission coefficient (κ) is the one that depends on the viscosity. Hence, we calculated κ at different solvent viscosities using two different methods: **Grote-Hynes Theory** (GHT) and **reactive flux formalism** (RF) and fitted it to the following heuristic relation to find α.

$$\frac{\kappa}{\kappa_0} = \left(\frac{\eta}{\eta_0}\right)^{-\alpha} \tag{18}$$

1. Grote-Hynes Theory (GHT)

GHT expresses the transmission coefficient as the ratio of the reactive frequency (λ_r) to the barrier frequency (ω_b)[19].

$$\kappa_{GH} = \frac{\lambda_r}{\omega_b} \tag{19}$$

The reactive frequency is the measure of the actual rate of passage across the barrier and can be obtained by solving the self-consistent equation:

$$\lambda_r^2 - \omega_b^2 + \lambda_r \hat{\xi}(\lambda_r) = 0, \tag{20}$$

where $\hat{\xi}(\lambda_r)$ is the effective friction experienced by the reaction coordinate and can be expressed as,

$$\hat{\xi}(\lambda_r) = \int_0^\infty e^{-\lambda_r t}\xi(t)dt \tag{21}$$

The barrier frequency ω_b can be calculated from the curvature of the potential, using the double derivative with respect to the reaction coordinate q at the Transition State (TS):

$$\omega_b = \sqrt{\frac{1}{\mu}\left|\frac{\partial^2 V}{\partial q^2}\right|_{TS}} \tag{22}$$

In the high friction overdamped limit, the effective friction in equation (20) is replaced by the zero-frequency friction ξ, which reduces the GHT transmission coefficient to the KT expression:

$$\kappa_{Kr} = \frac{\omega_b}{\xi} \tag{23}$$

2. Reactive Flux Formalism (RF)

For systems with very high barrier heights, that is, $E_b >> k_B T$, the barrier-crossing process becomes a rare event. In such cases, it becomes impractical and computationally expensive to follow the system from the reactant well to the product well. Hence, calculating MFPT in such cases is not an option. For this reason, Chandler and coworkers devised the RF formalism[34], where we place the system in the transition state and propagate trajectories both forward and backward in time. If the trajectories end up in the reactant well in backward time and in the product well in forward time, they are labeled as RP trajectories. Similarly, if they ended up in the product well in backward time and the reactant well in forward time, they are labeled as PR trajectories. However, the trajectories that ended up in the same well in both forward and backward time are the recrossed trajectories. They are labeled as RR or PP depending on their initial and final basins.

Once we have labeled the trajectories, we can calculate the Reactive Flux transmission coefficient κ_{RF}, which is the ratio of the actual rate (where both positive and negative flux contribute) to the TST rate (where only the positive flux contributes)[35].

$$\kappa_{RF} = \frac{\sum_{i,+}^N \omega_i |v_i| Q_i - \sum_{i,-}^N \omega_i |v_i| Q_i}{\sum_{i,\pm}^N \omega_i |v_i| Q_i} \tag{24}$$

Here, "+" represents trajectories that have initial positive flux, and "−" represents trajectories with initial negative flux. v_i is the velocity of the reaction coordinate at the TS for the i-th trajectory. ω_i is the probability of the trajectory to have the i^{th} initial configuration i.e., $e^{-V(q_i^0)/k_B T}$ (where q_i^0 is the zero-time value of the reaction coordinate). Q_i is assigned as:

$$Q_i = \begin{cases} +1 & \text{if R} \longrightarrow \text{P} \\ 0 & \text{if R} \longrightarrow \text{R or P} \longrightarrow \text{P} \\ -1 & \text{if P} \longrightarrow \text{R} \end{cases} \tag{25}$$

The barrier is relatively low ($\sim 3k_B T$) for both

our systems, which allows us to calculate the MFPT quite easily. Nevertheless, we use the Reactive Flux method to obtain an additional numerical estimate of barrier-crossing rates. We then compare these numerical estimates with results from GHT, which provides an analytical estimate of the rate based on a non-Markovian description of the RC motion.

IV. RESULTS AND DISCUSSIONS

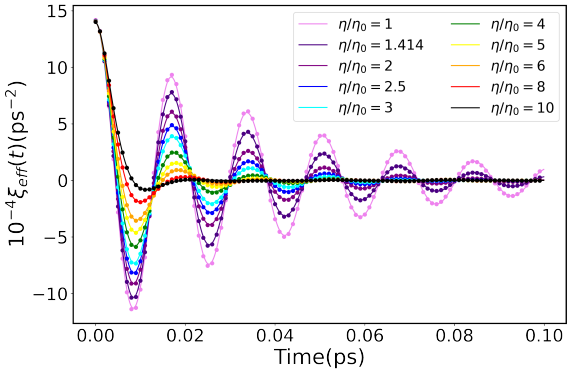

FIG. 2: Memory kernels $\xi_{eff(t)}$ from the diatom model for different scaled viscosity values η/η_0.

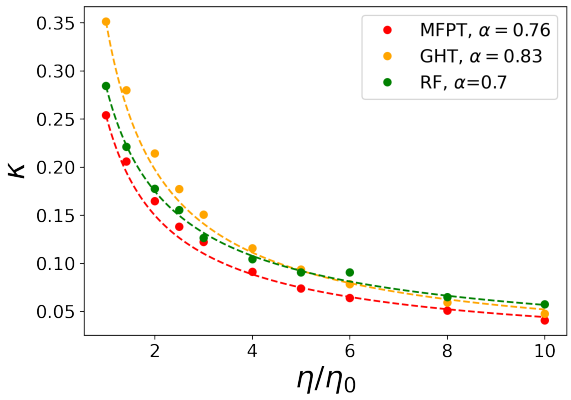

FIG. 3: Variation of Transmission Coefficients κ extracted using MFPT, GHT, and RF with scaled viscosity η/η_0.

A. Model Diatomic System

We showcase the memory kernels for the diatomic model for different relative viscosities η/η_0 in Figure 2. The excellent agreement between the kernels extracted from the MD simulations (dotted lines) and the analytical kernels $\xi_{eff}(t)$ (solid lines) derived in Equation (11) confirms the presence of memory effects in our system.

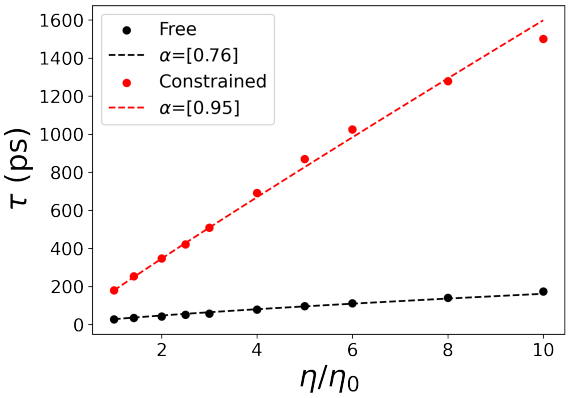

FIG. 4: Variation of MFPT values with scaled viscosity η/η_0 for the Free and Constrained diatom model.

We compute the GHT transmission coefficients (κ_{GH}) using the memory kernels extracted from the MD simulations. We then compared these coefficients with both the RF and the MFPT transmission coefficients. The MFPT TCs were determined as

$$\kappa_{MFPT} = \frac{k}{k_{TST}} = \frac{1}{\tau k_{TST}}, \tag{26}$$

where k is the rate, k_{TST} represents the Transition State Theory rate, and τ denotes the MFPT. Figure 3 shows the values of α obtained by fitting the TCs to Equation (18). We find that the α values are less than one for all three methods, which suggests a fractional viscosity dependence and, hence, a deviation from Kramers' theory. Both of these behaviors are usually considered to indicate the presence of an Internal Friction. However, we must remember that GHT is a non-Markovian rate theory that accounts for memory effects, whereas RF and MFPT provide direct numerical estimates. The close alignment of the GHT α values with those from RF and MFPT implies that the observed fractional viscosity dependence likely stems from the inherent memory effects in our model.

Figure 4 shows the MFPT values at different viscosities for the diatom model. We compare two scenarios: a Markovian limit (marked as Constrained) and a non-Markovian limit (marked as Free). We constrain the motion of the reaction coordinate (RC) to reach the Markovian limit by slowing its diffusion timescale τ_D (where $\tau_D = L^2\xi/k_BT$) following the work of Kappler and Daldrop[36]. For the diatom model, we slow down the diffusion of the particle 'B' by increasing the mass of the free particle 'A'. The purpose of this exercise is to show that when the reaction coordinate diffuses much slower than the memory time τ_Γ (where $\tau_\Gamma = 1/\xi$), the memory effects do not come into play, and the system experiences largely

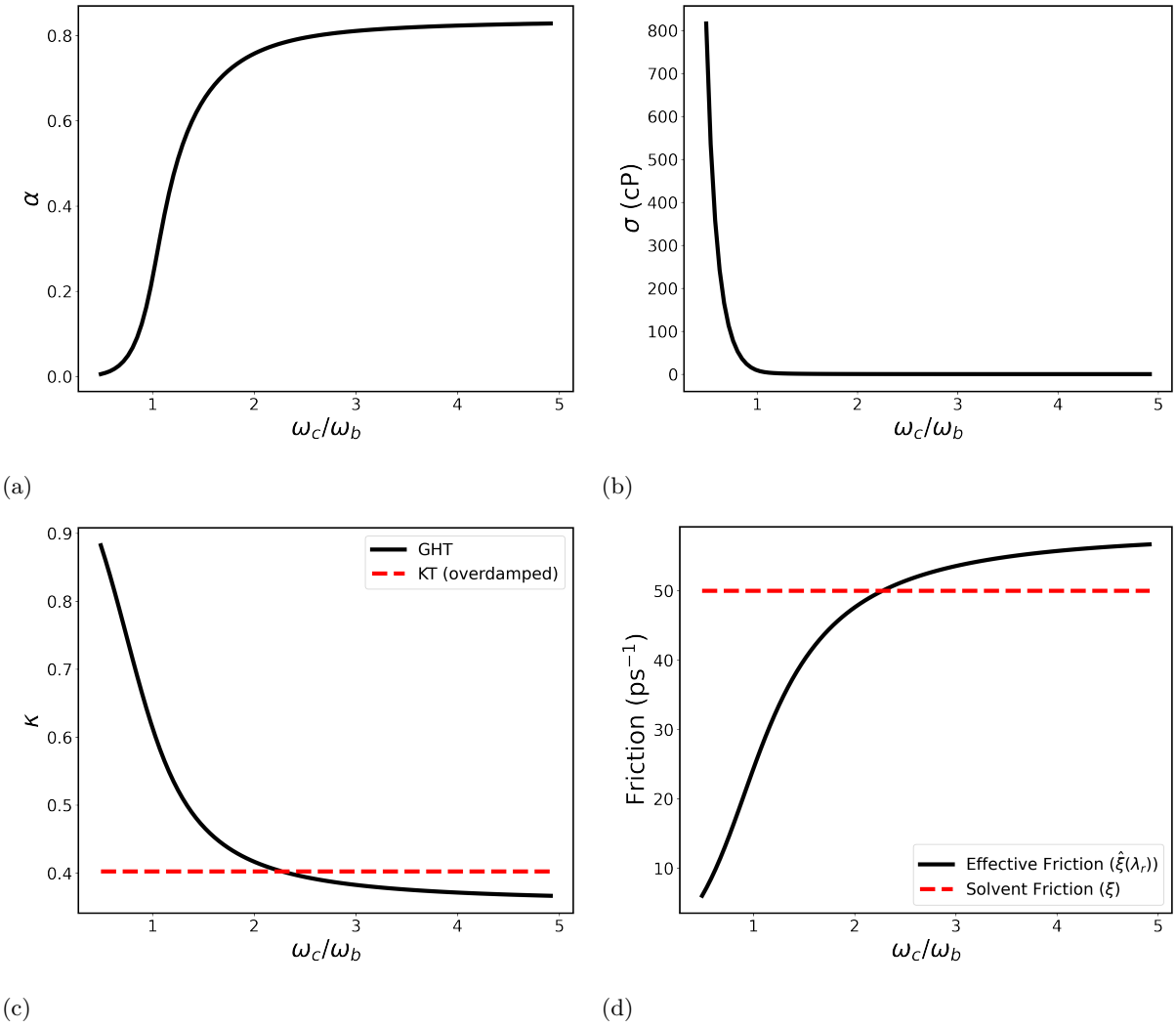

FIG. 5: Variation of (a) power-law exponent α and (b) Ansari's fit parameter σ with relative coupling strength (ω_c /ω_b). Variation of (c) Transmission Coefficients κ and (d) Friction with relative coupling strength (ω_c /ω_b) at a fixed viscosity of 1 cP.

a Markovian friction. As expected, we see in Figure 4 that for the constrained system, the relative MFPT values τ/τ_o scale almost linearly with the relative viscosity η/η_0. The α value from fitting to the equation (12) is found to be close to unity, demonstrating a close adherence to Kramer's theory. The free system, on the other hand, deviates strongly from Kramers' theory, with an α value much lower than unity. This is in line with existing observations in the literature that memory effects only become prominent when the RC motion is very fast.

Note how the MFPT values in Figure 4 are much lower for the free system than the corresponding values for the constrained system. Since the rate is the inverse of the MFPT, it suggests that the free system crosses the barrier faster than the constrained system. This is a frequently overlooked aspect in the literature on Internal Friction that the rates, while lowered from the TST estimate, are still greater than those expected from Kramer's Theory (Constrained model), i.e., $k_{Kr} < k < k_{TST}$.

Previously we had observed a fractional viscosity dependence of rates for a single particle crossing a one-dimensional barrier in the presence of explicit solvent molecules[21]. We also showed that the same model adhered closely to KT (with $\alpha \simeq 1$) in absence of explicit solvent molecules, thereby proving that the memory effects arising from correlated solute-solvent motion were responsible for the deviations from KT. In contrast, the diatom model considered presently lacks any explicit solvent molecules while having an additional internal coordinate. So we cannot attribute the fractional viscosity dependence indicated by both MFPT and TC results to solvent memory effects. Instead, the memory friction that arises from the coupling of the RC to an orthogonal degree of freedom is responsible for the fractional viscosity dependence.

This shows that memory effects need not arise from coupled solute-solvent motion from outside the molecule; they can also emerge from within the system.

B. Barrier Curvature and Coupling Strength Dependence

We can see from the definition of the transmission coefficient from GHT that it explicitly depends on the barrier curvature through ω_b. On the other hand, the reactive frequency λ_r depends on the memory kernel $\xi_{eff}(t)$, which in this case is characterized by two parameters: coupling strength ω_c and static solvent friction ξ. We show in figure S2 in the supplementary material how λ_r increasingly diverges from the barrier frequency ω_b with increasing ω_c. Hence, we expect that the fractional viscosity dependence of the rate of the diatom model will also depend on these factors. In this subsection, we explore the variation of the fractional viscosity dependence (characterized by α and σ) with ω_b and ω_c. However, the number of simulations required would be too large and computationally expensive. So, we use the analytical kernel in equation (11) to calculate TC from GHT. For each pair of ω_c, ω_b values, we calculate the GHT TC over a range of viscosity values and fit them to both the power law $\kappa/\kappa_0 = (\eta_0/\eta)^\alpha$ and Ansari's equation $\kappa = C^{'}/(\eta+\sigma)$ to extract the fit parameters α and σ respectively. We summarize the results in Figure 5.

Both Figures 5a and 5b (or Figures S1a and S1b in the supplementary material) indicate that the fractional viscosity dependence becomes more prominent at higher barrier curvatures and lower coupling strengths. A fractional viscosity dependence means that the reaction coordinate is either not experiencing the full solvent friction or is experiencing additional friction on top of the solvent friction. This is evident from Figure 5c. Initially, for weak coupling ($\omega_c < \omega_b$), the GHT TC is larger than the Kramers Theory estimate, suggesting that the RC does not experience the full solvent friction ξ. Instead, it experiences, according to GHT, an effective frequency-dependent friction $\hat{\xi}(\lambda_r)$ that is defined as $\hat{\xi}(\lambda_r) = \int_0^\infty e^{-\lambda_r t}\xi_{eff}(t)dt$. We show in Figure 5d that this effective friction is smaller than the solvent friction ξ because the RC crosses the barrier much faster than the slow oscillations in $\xi_{eff}(t)$. Conversely, for stronger coupling($\omega_c > \omega_b$), the oscillations slightly increase effective friction beyond solvent friction ξ so that the GHT TC falls below the Kramers Theory estimate.

We would like to highlight that this is consistent with our previous findings for a single particle[21], where α was found to increase and σ to decrease with the solute-solvent coupling parameter ϵ/ϵ_0. It is clear that we cannot attribute the enhanced fractional viscosity dependence to any static friction arising from the interior of the molecule in this model. If that were indeed the case, α and σ would have remained unchanged with the coupling. Also note how Ansari's fit parameter σ is abnormally large for low coupling strength where the solvent friction is suppressed, making its interpretation as an additional internal friction questionable.

C. Butane Dihedral Rotation

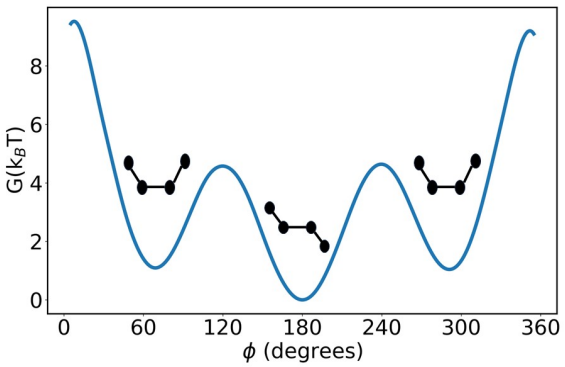

FIG. 6: One-dimensional Free Energy surface of Butane dihedral rotation.

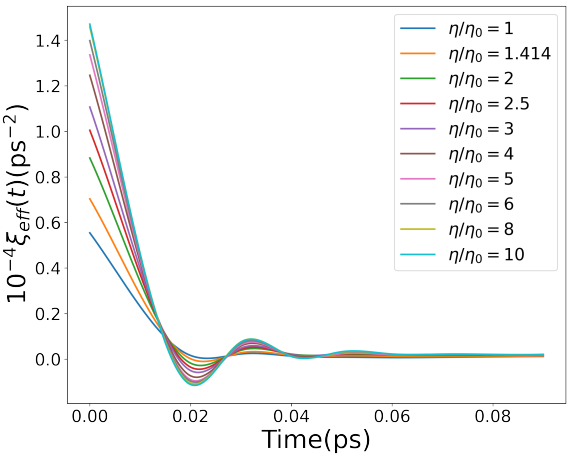

FIG. 7: Memory Kernels $\xi_{eff}(t)$ extracted from MD simulation trajectories of butane for different scaled viscosities η/η_0.

Butane isomerizes from a less stable gauche to a more stable anti-conformer. This conformational change can be entirely characterized by a change in the dihedral angle ϕ, as shown by the free energy surface of the butane dihedral rotation in Figure 6. The memory kernels extracted from the bu-

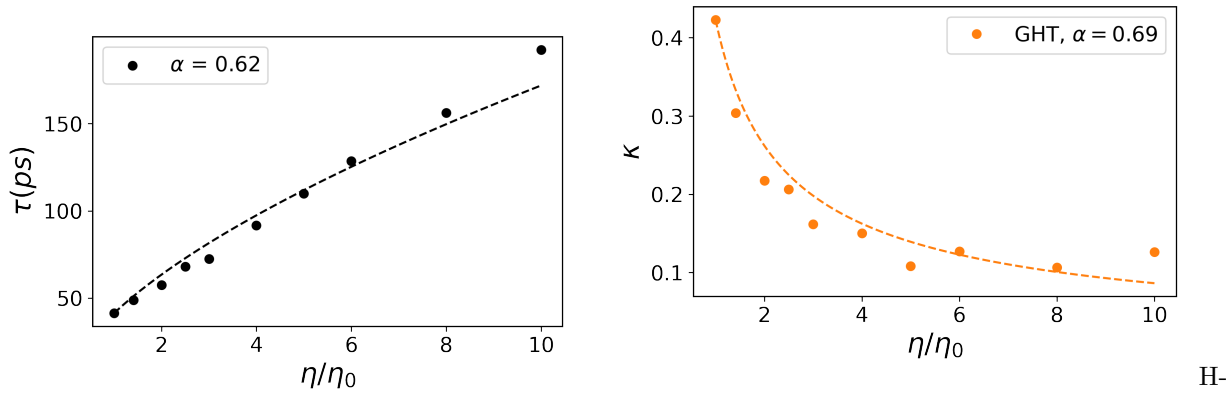

(a) (b)

FIG. 8: (a) MFPT values τ and (b) GHT Transmission Coefficient κ against scaled viscosities η/η_0 for Butane.

tane simulations at different viscosities are shown in Figure 7 after interpolation.

Like with the diatom model, we calculated the MFPT for the dihedral rotation of butane from the Gauche conformer to the anti-conformer. Figure 8a shows that the MFPT values do not vary linearly with viscosity. We find the fractional viscosity dependence α by fitting the MFPT values to Eq. (12) to be equal to 0.62, suggesting a deviation from Kramers' behavior. A similar α value of 0.69 is also obtained by fitting the Grote-Hynes transmission coefficients at different viscosities, as shown in Figure 8b. This suggests that the fractional viscosity dependence and deviation from Kramers' behavior in a realistic system like Butane can also be attributed to the presence of memory effects.

The dihedral angle in butane is coupled to six orthogonal degrees of freedom: three translational and three orientational[22]. So, we can use our simple diatomic model to explain the memory effects in butane dihedral rotation. For this purpose, we fit the butane memory kernels to our analytical expression in (11) and optimize the adjustable parameters ω and ξ. However, we find that the fit is quite poor (see Figure S3a in the supplementary material). Therefore, we fitted it using three adjustable parameters ω, ξ, and γ to find a much better fit (see Figure S3b in the supplementary material). Since γ serves as an effective oscillation frequency in our model emerging from an interplay between the coupling frequency ω and the friction coefficient ξ, it might seem odd to use it as an adjustable parameter. But for a complex reaction coordinate such as the dihedral angle, γ may not have such a simple definition since we are approximating the six orthogonal degrees of freedom as a single effective orthogonal coordinate. The fitted kernel yields a GHT TC value of 0.44, which is quite close to the GHT TC value of 0.41 that we

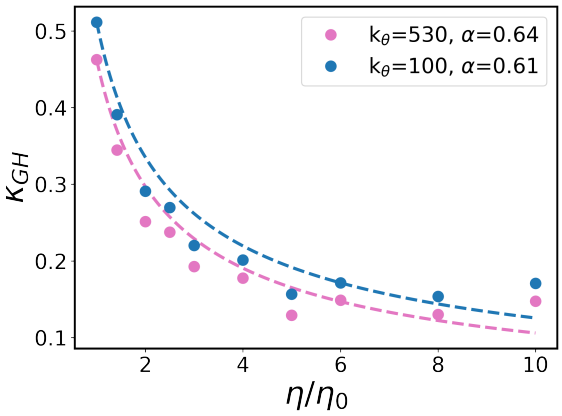

FIG. 9: Variation of GHT TC with scaled viscosity η/η_0 for different bond-angle force constants k_θ

obtained from the memory kernel extracted from MD simulations.

We altered the coupling of the dihedral angle to the orthogonal degrees of freedom by modulating the fluctuations of the bond angle using a harmonic potential $V(\theta)$ as given below.

$$V(\theta) = \frac{1}{2}k_\theta(\theta - \theta_0)^2 \tag{27}$$

Here k_θ is the force constant, and θ_0 is the equilibrium value of the bond angle. We make the bond angle more flexible by lowering k_θ from 530 kJ mol^{-1} rad $^{-2}$ to 100 kJ mol^{-1} rad $^{-2}$. Enhanced fluctuations in the bond angle led to a weaker coupling of the atomic motions with the dihedral angle. We confirmed this by fitting the memory kernels extracted from MD simulations. The fitted coupling frequency ω_c decreases from 72.92 ps^{-1} to 71.16 ps^{-1}(see Figures S4a and S4b

in the supplementary material). As expected from our analytical model, we found in Figure 9 that a weaker coupling resulted in a lower α value, indicating a greater fractional viscosity dependence. The carbon atoms experience the solvent friction directly but are unable to relay it to the dihedral angle to its full extent. We validated this by calculating the effective friction $\hat{\xi}(\lambda_r)$ which drops from 47.6 ps^{-1} to 45.1 ps^{-1}. With weaker coupling, the solvent friction contribution decreases. This qualitatively shows that the discussions from the previous section apply to butane dihedral rotation as well.

V. CONCLUSION

Non-Markovian friction has attracted significant attention in recent times to explain the anomalous rates of biophysical barrier-crossing processes[37,38]. In the present work, we have illustrated with a diatom model and butane how such memory effects can arise in the simplest of molecules due to the coupling of motions between a reactive mode and orthogonal non-reactive modes. We confirmed this by calculating transmission coefficients using multiple methods along with the direct rate calculation using MFPT.

In particular, we show that the barrier curvature (ω_b) and the coupling strength (ω_c) play a critical role in modulating the nature of memory effects. For the single-particle model we previously considered[21], the solvent friction was suppressed due to non-equilibrium solvation by explicit solvent molecules. However, for the diatom model considered here, we find that the memory effects switch from suppressing the solvent friction to supplementing it, depending on the coupling strength relative to the barrier frequency. The suppression of solvent friction in the low-coupling limit can be thought of as the solvent friction being transmitted partially to the reaction coordinate by the orthogonal degrees of freedom.

Although the above insights were inferred for a simple model system, we show that they can be extended to realistic systems like butane as well. By fitting memory kernels extracted from MD simulations to our analytically derived kernel, we could determine the frequency ω_c with which the reaction coordinate was coupled to orthogonal non-reactive modes. This allowed us to predict the extent of fractional viscosity dependence expected from barrier-crossing rates in such systems. We suspect that the experimentally observed factors usually responsible for internal friction, such as concerted dihedral rotations[5,17], non-native hydrogen bonding[10], increased dispersion interactions[18], etc., might be operating through a combination of solvent and internal memory effects in complex biological systems like proteins. In such cases, the decoupling of the two effects and the accurate identification of the source of the fractional viscosity dependence remain a difficult challenge, which we hope to address in the future.

SUPPLEMENTARY MATERIAL

The Supplementary Material contains 3D plots describing the variation of α and σ with the coupling strength and barrier frequency, a plot of the reactive frequency against ω_c/ω_b and the fitting of the memory kernels extracted from MD simulations of Butane.

ACKNOWLEDGEMENTS

The authors acknowledge the support and resources provided by the 'PARAM Brahma Facility' under the National Supercomputing Mission, Government of India at the Indian Institute of Science Education and Research, Pune. The Department of Biotechnology (DBT), India (BT/PR34215/AI/133/22/2019) is acknowledged for partial funding support. The authors acknowledge Dr. James.T. Hynes for extensive discussions.

AUTHOR DECLARATIONS

Conflict of Interest

The authors have no conflicts to disclose.

Author Contributions

Bikirna Roy: Conceptualization (equal); Methodology (lead); Writing - original draft (lead); Writing - review & editing (equal). **Hridya V. M. :** Conceptualization (equal); Methodology (supporting). **Arnab Mukherjee:** Conceptualization (equal); Writing - original draft (supporting); Writing - review & editing (equal).

DATA AVAILABILITY

The data that support the findings of this study are openly available in `https://github.com/arnabpune/memory_friction`.

REFERENCES

[1] H.A. Kramers. Brownian motion in a field of force and the diffusion model of chemical reactions. *Physica*, 7(4):284–304, 1940.

[2]Stephan P. Velsko, David H. Waldeck, and Graham R. Fleming. Breakdown of Kramers theory description of photochemical isomerization and the possible involvement of frequency dependent friction. *The Journal of Chemical Physics*, 78(1):249–258, 01 1983.

[3]Anjum Ansari, Colleen M. Jones, Eric R. Henry, James Hofrichter, and William A. Eaton. The role of solvent viscosity in the dynamics of protein conformational changes. *Science*, 256(5065):1796–1798, 1992.

[4]Andrea Soranno, Brigitte Buchli, Daniel Nettels, Ryan R. Cheng, Sonja Müller-Späth, Shawn H. Pfeil, Armin Hoffmann, Everett A. Lipman, Dmitrii E. Makarov, and Benjamin Schuler. Quantifying internal friction in unfolded and intrinsically disordered proteins with single-molecule spectroscopy. *Proceedings of the National Academy of Sciences*, 109(44):17800–17806, 2012.

[5]Debapriya Das, Lisha Arora, and Samrat Mukhopadhyay. Short-range backbone dihedral rotations modulate internal friction in intrinsically disordered proteins. *Journal of the American Chemical Society*, 144(4):1739–1747, 2022. PMID: 35068142.

[6]Andrea Soranno, Andrea Holla, Fabian Dingfelder, Daniel Nettels, Dmitrii E. Makarov, and Benjamin Schuler. Integrated view of internal friction in unfolded proteins from single-molecule fret, contact quenching, theory, and simulations. *Proceedings of the National Academy of Sciences*, 114(10):E1833–E1839, 2017.

[7]Troy Cellmer, Eric R. Henry, James Hofrichter, and William A. Eaton. Measuring internal friction of an ultrafast-folding protein. *Proceedings of the National Academy of Sciences*, 105(47):18320–18325, 2008.

[8]Linlin Qiu and Stephen J. Hagen. Internal friction in the ultrafast folding of the tryptophan cage. *Chemical Physics*, 307(2):243–249, 2004. The Physics of Protein Folding and Function.

[9]David De Sancho, Anshul Sirur, and Robert B Best. Molecular origins of internal friction effects on protein-folding rates. *Nature communications*, 5(1):4307, 2014.

[10]Julius C. F. Schulz, Markus S. Miettinen, and R. R. Netz. Unfolding and folding internal friction of -hairpins is smaller than that of -helices. *The Journal of Physical Chemistry B*, 119(13):4565–4574, 2015. PMID: 25741584.

[11]Beth G Wensley, Sarah Batey, Fleur AC Bone, Zheng Ming Chan, Nuala R Tumelty, Annette Steward, Lee Gyan Kwa, Alessandro Borgia, and Jane Clarke. Experimental evidence for a frustrated energy landscape in a three-helix-bundle protein family. *Nature*, 463(7281):685–688, 2010.

[12]Beth G. Wensley, Lee Gyan Kwa, Sarah L. Shammas, Joseph M. Rogers, and Jane Clarke. Protein folding: Adding a nucleus to guide helix docking reduces landscape roughness. *Journal of Molecular Biology*, 423(3):273–283, 2012.

[13]Lee Gyan Kwa, Beth G. Wensley, Crispin G. Alexander, Stuart J. Browning, Benjamin R. Lichman, and Jane Clarke. The folding of a family of three-helix bundle proteins: Spectrin r15 has a robust folding nucleus, unlike its homologous neighbours. *Journal of Molecular Biology*, 426(7):1600–1610, 2014.

[14]Wenwei Zheng, David De Sancho, Travis Hoppe, and Robert B. Best. Dependence of internal friction on folding mechanism. *Journal of the American Chemical Society*, 137(9):3283–3290, 2015. PMID: 25721133.

[15]Gouri S. Jas, William A. Eaton, and James Hofrichter. Effect of viscosity on the kinetics of -helix and -hairpin formation. *The Journal of Physical Chemistry B*, 105(1):261–272, 2001.

[16]Christopher A. Ross and Michelle A. Poirier. Protein aggregation and neurodegenerative disease. *Nature Medicine*, 10(7):S10–S17, Jul 2004.

[17]Ignacia Echeverria, Dmitrii E. Makarov, and Garegin A. Papoian. Concerted dihedral rotations give rise to internal friction in unfolded proteins. *Journal of the American Chemical Society*, 136(24):8708–8713, 2014. PMID: 24844314.

[18]Pulikallu Sashi, Dasari Ramakrishna, and Abani K. Bhuyan. Dispersion forces and the molecular origin of internal friction in protein. *Biochemistry*, 55(33):4595–4602, 2016. PMID: 27479029.

[19]Richard F. Grote and James T. Hynes. The stable states picture of chemical reactions. II. Rate constants for condensed and gas phase reaction models. *The Journal of Chemical Physics*, 73(6):2715–2732, 07 2008.

[20]Biman Bagchi and David W. Oxtoby. The effect of frequency dependent friction on isomerization dynamics in solution. *The Journal of Chemical Physics*, 78(5):2735–2741, 03 1983.

[21]V. M. Hridya and Arnab Mukherjee. Probing the viscosity dependence of rate: Internal friction or the lack of friction? *The Journal of Physical Chemistry B*, 122(39):9081–9086, 2018. PMID: 30205686.

[22]Jan O. Daldrop, Julian Kappler, Florian N. Brünig, and Roland R. Netz. Butane dihedral angle dynamics in water is dominated by internal friction. *Proceedings of the National Academy of Sciences*, 115(20):5169–5174, 2018.

[23]Kirill Zinovjev, Paul Guénon, Carlos A. Ramos-Guzmán, J. Javier Ruiz-Pernía, Damien Laage, and Iñaki Tuñón. Activation and friction in enzymatic loop opening and closing dynamics. *Nature Communications*, 15(1):2490, Mar 2024.

[24]G. van der Zwan and James T. Hynes. Reactive paths in the diffusion limit. *The Journal of Chemical Physics*, 77(3):1295–1301, 1982.

[25]Bradley J. Gertner, Kent R. Wilson, and James T. Hynes. Nonequilibrium solvation effects on reaction rates for model sn2 reactions in water. *The Journal of Chemical Physics*, 90(7):3537–3558, 1989.

[26]A. P. Thompson, H. M. Aktulga, R. Berger, D. S. Bolintineanu, W. M. Brown, P. S. Crozier, P. J. in 't Veld, A. Kohlmeyer, S. G. Moore, T. D. Nguyen, R. Shan, M. J. Stevens, J. Tranchida, C. Trott, and S. J. Plimpton. LAMMPS - a flexible simulation tool for particle-based materials modeling at the atomic, meso, and continuum scales. *Comp. Phys. Comm.*, 271:108171, 2022.

[27]T. Schneider and E. Stoll. Molecular-dynamics study of a three-dimensional one-component model for distortive phase transitions. *Phys. Rev. B*, 17:1302–1322, Feb 1978.

[28]Berk Hess, Carsten Kutzner, David van der Spoel, and Erik Lindahl. Gromacs 4: algorithms for highly efficient, load-balanced, and scalable molecular simulation. *Journal of Chemical Theory and Computation*, 4(3):435–447, 2008. PMID: 26620784.

[29]Maria M. Reif, Moritz Winger, and Chris Oostenbrink. Testing of the gromos force-field parameter set 54a8: Structural properties of electrolyte solutions, lipid bilayers, and proteins. *Journal of Chemical Theory and Computation*, 9(2):1247–1264, 2013. PMID: 23418406.

[30]Berk Hess, Henk Bekker, Herman J. C. Berendsen, and Johannes G. E. M. Fraaije. Lincs: A linear constraint solver for molecular simulations. *Journal of Computational Chemistry*, 18(12):1463–1472, 1997.

[31]V. M. Hridya, James T. Hynes, and Arnab Mukherjee. Dynamical recrossing in the intercalation process of the anticancer agent proflavine into dna. *The Journal of Physical Chemistry B*, 123(51):10904–10914, 2019. PMID: 31671261.

[32]B. J. Berne and G. D. Harp. *On the Calculation of Time Correlation Functions*, pages 63–227. John Wiley Sons, Ltd, 1970.

[33]Peter Hänggi, Peter Talkner, and Michal Borkovec. Reaction-rate theory: fifty years after kramers. *Rev. Mod. Phys.*, 62:251–341, Apr 1990.

[34]David Chandler. Statistical mechanics of isomerization dynamics in liquids and the transition state approximation. *The Journal of Chemical Physics*, 68(6):2959–2970, 1978.

[35]Scott H. Northrup and James T. Hynes. The stable states picture of chemical reactions. i. formulation for rate constants and initial condition effects. *The Journal of Chemical Physics*, 73(6):2700–2714, 1980.

[36]Julian Kappler, Jan O. Daldrop, Florian N. Brünig, Moritz D. Boehle, and Roland R. Netz. Memory-induced acceleration and slowdown of barrier crossing. *The Journal of Chemical Physics*, 148(1):014903, 01 2018.

[37]Cihan Ayaz, Lucas Tepper, Florian N. Brünig, Julian Kappler, Jan O. Daldrop, and Roland R. Netz. Non-markovian modeling of protein folding. *Proceedings of the National Academy of Sciences*, 118(31):e2023856118, 2021.

[38]Benjamin A. Dalton, Cihan Ayaz, Henrik Kiefer, Anton Klimek, Lucas Tepper, and Roland R. Netz. Fast protein folding is governed by memory-dependent friction. *Proceedings of the National Academy of Sciences*, 120(31):e2220068120, 2023.